

APATITE CHEMISTRY AS A POSSIBLE INDICATOR OF MINERALIZATION AT THE GRANULITE-FACIES METAMORPHOSED TAMPIA GOLD DEPOSIT

JK Porter and P Duuring





Department of **Energy, Mines,
Industry Regulation and Safety**

REPORT 251

APATITE CHEMISTRY AS A POSSIBLE INDICATOR OF MINERALIZATION AT THE GRANULITE-FACIES METAMORPHOSED TAMPIA GOLD DEPOSIT

JK Porter^{1,2}, P Duuring

1 MinEx CRC, 26 Dick Perry Ave, Kensington WA 6151

2 Future Industries Institute, University of South Australia, Mawson Lakes SA 5095

PERTH 2024



**Geological Survey of
Western Australia**

MINISTER FOR MINES AND PETROLEUM
Hon David Robert Michael MLA

DIRECTOR GENERAL, DEPARTMENT OF ENERGY, MINES, INDUSTRY REGULATION AND SAFETY
Richard Sellers

EXECUTIVE DIRECTOR, GEOLOGICAL SURVEY AND RESOURCE STRATEGY
Michele Spencer

REFERENCE

The recommended reference for this publication is:

Porter, JK and Duuring, P 2024, Apatite chemistry as a possible indicator of mineralization at the granulite-facies metamorphosed Tampia gold deposit: Geological Survey of Western Australia, Report 251, 19p.

ISBN 978-1-76148-043-0

ISSN 2204-4345



A catalogue record for this book is available from the National Library of Australia

Grid references in this publication refer to the Geocentric Datum of Australia 1994 (GDA94). Locations mentioned in the text are referenced using Map Grid of Australia 1994 (MGA94) coordinates, Zone 50. All locations are quoted to at least the nearest 100 m.



About this publication

The study presented in this Report is the result of a collaborative research project: Detection of Distal Footprints of Minerals Systems in the Southwest of Western Australia: Linking Basement and Cover (SOWETO), with the Geological Survey of Western Australia (GSWA), CSIRO, the Minerals Research Institute of Western Australia (MRIWA), Anglo American Ltd and Ramelius Resources Ltd. The principal objective of this research is to build a contextual framework to help more efficient mineral exploration protocols in the southwest region of Western Australia. This research aims to better understand how the basement and cover variability of the area are linked, and how these links can be used to vector mineral systems at depth and in the cover.

The TESCAN Integrated Mineral Analyser (TIMA) instrument was funded by a grant from the Australian Research Council (LE140100150) and is operated by the John de Laeter Centre (JdLC) at Curtin University with the support of the GSWA, The University of Western Australia and Murdoch University.

Disclaimer

This product uses information from various sources. The Department of Energy, Mines, Industry Regulation and Safety (DEMIRS) and the State cannot guarantee the accuracy, currency or completeness of the information. Neither the department nor the State of Western Australia nor any employee or agent of the department shall be responsible or liable for any loss, damage or injury arising from the use of or reliance on any information, data or advice (including incomplete, out-of-date, incorrect, inaccurate or misleading information, data or advice) expressed or implied in, or coming from, this publication or incorporated into it by reference, by any person whatsoever.

Acknowledgement of Country

We respectfully acknowledge Aboriginal peoples as the Traditional Custodians of this land on which we deliver our services to the communities throughout Western Australia. We acknowledge their enduring connection to the lands, waterways and communities and pay our respects to Elders past and present.

Published 2024 by the Geological Survey of Western Australia

This Report is published in digital format (PDF) and is available online at <www.demirs.wa.gov.au/GSWApublications>.



© State of Western Australia (Department of Energy, Mines, Industry Regulation and Safety) 2024

With the exception of the Western Australian Coat of Arms and other logos, and where otherwise noted, these data are provided under a Creative Commons Attribution 4.0 International Licence.
(<https://creativecommons.org/licenses/by/4.0/legalcode>)

Further details of geoscience products are available from:

First Floor Counter
Department of Energy, Mines, Industry Regulation and Safety
100 Plain Street
EAST PERTH WESTERN AUSTRALIA 6004
Telephone: +61 8 9222 3459 Email: publications@demirs.wa.gov.au
www.demirs.wa.gov.au/GSWApublications

Cover image

Hand specimen of gold ore from the Tampia deposit, featuring a coarse-grained leucosome in mafic gneiss, enriched in pyrrhotite

Contents

Scientific abstract.....	1
Lay abstract	1
Introduction.....	2
Geological context.....	2
Methods	2
Sample selection.....	2
TIMA	3
EPMA	4
LA-ICP-MS	5
Results.....	5
Apatite morphology and mineral associations	5
Sample 239980, mafic gneiss	5
Samples 239979B and 239981, mineralized leucosomes in mafic gneiss.....	5
Sample 239984, mineralized leucosome in mafic gneiss	9
Samples 239996 and 240032, mineralized samples from other drillholes.....	9
Apatite chemistry.....	9
Samples 239980, 239979B, 239981	9
Sample 239984	10
Samples 239996 and 240032	10
Discussion.....	12
Apatite as an indicator of host rock compositional variability	12
Evaluating apatite's utility in identifying gold mineralization	12
Comparison of Tampia apatite with regional apatite compositions	15
Conclusions	17
Acknowledgements.....	17
References	18

Appendices

Available with the PDF online as an accompanying digital resource

1. Drillhole locations
2. Apatite compositional data, EPMA
3. Apatite compositional data, LA-ICP-MS
4. Sample summaries
5. Sample descriptions

Figures

1. Tampia gold deposit geology map with drillhole locations.....	3
2. Photographs of mafic gneiss with gold-bearing examples.....	4
3. TIMA images showing textural differences in mafic gneiss.....	6
4. Photomicrographs of apatite grains in mafic gneiss.....	8
5. REE and Y concentration trends in apatite from mafic gneiss.....	10
6. Apatite composition discrimination in mafic gneiss using binary plots	11
7. Apatite source discrimination graph showing Sr/Y vs sum LREE	12
8. Binary plots for apatite compositions in mafic gneiss.....	13
9. Geochemistry of mafic gneiss at Tampia showing element ratios	14
10. Apatite chemistry in mineralization potential discrimination plot	16
11. Rock fertility discrimination plot of the Yilgarn Craton.....	16

Apatite chemistry as a possible indicator of mineralization at the granulite-facies metamorphosed Tampia gold deposit

JK Porter^{1,2}, P Duuring

Scientific abstract

The study presented in this Report investigates the utility of apatite chemistry as a discriminant for mineralization within granulite-facies metamorphosed terranes, with a focus on the Tampia gold deposit in the Youanmi Terrane of the Yilgarn Craton, Western Australia. The primary aim was to assess whether apatite chemistry can serve as a reliable tool for identifying gold mineralization in such complex geological settings. To this end, apatite grains from typical mafic gneiss and those associated with obvious mineralization were analysed and compared against both global and regional apatite chemistry databases, including those associated with intrusion-related gold deposits within the Yilgarn and Pilbara Cratons.

Our findings reveal that the chemistry of apatite at Tampia closely mirrors the compositional variations of its host rocks. Comparable chondrite normalized rare earth element (REE) multi-element trends, Eu, Ce and Y anomalies, and trace element abundances for Cl, F, Sr and Mn were observed between wallrock and more mineralized samples, indicating near-identical apatite chemistry trends for samples originating from the same precursor rock. However, apatite from vein- and leucosome-bearing, mineralized samples at Tampia did not exhibit distinguishable chemistry from typical gneiss samples analysed in this study. This suggests that: 1) apatite taken from typical gneiss and wallrock was also affected by mineralizing fluids and, therefore, cannot be used as chemical benchmarks for comparison with those from obvious mineralization; 2) apatite grains within the wallrock did not form during the gold mineralization event; or 3) any mineralization associated chemical signature in apatite was subsequently homogenized by barren, high-pressure–temperature metamorphic fluids.

Comparison of Tampia apatite with established global databases of major magmatic and hydrothermal ore deposits highlighted the challenges of categorizing Tampia apatite within existing frameworks due to mismatches in fertility indicators. These insights underscore the complexity of using apatite chemistry for mineral exploration in granulite-facies rocks and suggest a need for further refinement of geochemical databases to include a broader spectrum of deposit types and geological settings. Recommendations for future research include expanding the lithological scope of study samples to include apatite not affected by mineralizing fluids at Tampia, and conducting comparative analyses with similar gold deposits in the southwest Yilgarn Craton to further evaluate the predictive power of apatite chemistry in gold exploration.

KEYWORDS: apatite chemistry, mineral exploration, Tampia gold deposit

Lay abstract

This Report examines whether the mineral apatite can help explorers locate gold deposits in ancient rocks that have experienced high temperatures and pressures during granulite-facies regional metamorphism. Researchers assessed if the chemical makeup of apatite could indicate the presence of gold. They compared apatite from barren and gold-rich rocks at the Tampia gold deposit and analysed these patterns against known trends from other gold deposits worldwide. They found that while apatite chemistry reflects the type of rock it comes from, it does not clearly distinguish between gold-absent and gold-rich rocks.

¹ MinEx CRC, 26 Dick Perry Ave, Kensington WA 6151

² Future Industries Institute, University of South Australia, Mawson Lakes SA 5095

Introduction

Apatite is widely recognized for its utility in deducing the genesis and chemical composition of host rocks and is found across various rock types, spanning mafic to felsic igneous, metamorphic and sedimentary rocks, in both barren and mineralized environments (Sha and Chappell, 1999; Piccoli and Candela, 2002; Chu et al., 2009; Belousova et al., 2010; Cao et al., 2012). The occurrence of apatite in a broad spectrum of geological settings underscores its versatility in geological research.

The structure of apatite enables it to incorporate diverse elements under varying pressure–temperature (P – T) and oxygen fugacity (fO_2) conditions (Harlov, 2015; Hughes and Rakovan, 2015), providing critical insights into the fluids or melts involved in rock formation. This aspect is crucial for understanding the chemistry of the surrounding or source rocks and the nature of associated mineralization. Furthermore, owing to its resistance to mechanical transport, apatite liberated from its host rock can be transported and deposited in stream sediments, where it may serve as a geochemical marker for nearby bedrock (Mao et al., 2016; Gillespie et al., 2018; O'Sullivan et al., 2020) and any potential associated mineralization. This characteristic enhances the utility of apatite in geochemical exploration, including in the search for gold mineralization (Mao et al., 2016; Krneta et al., 2017; Xu et al., 2021).

Minerals in the apatite group are characterized by the general formula $M_5(TO_4)_3(A)$; typically, $Ca_5(PO_4)_3(F,Cl,OH)$, with a structure accommodating a wide range of periodic table elements. The A site in apatite commonly incorporates the halogens: F, Cl and OH, which act as proxies for fluids (Hughes and Rakovan, 2002; Hughes and Rakovan, 2015). They provide insights into the chemistry and conditions of rock-forming fluids, as well as rock source and type of associated mineralization. As these elements are comparatively mobile, they usually reflect the chemistry of the last fluid event that affected the apatite grains (Harlov, 2015).

In apatite, the primary cation sites, predominantly occupied by Ca, can be substituted by rare earth elements (REE) and various divalent metals, depending on their availability from host rocks and fluids, as well as formation conditions such as pressure, temperature and redox state (Harlov, 2015). As the primary phosphorus-bearing mineral in crustal rocks, the tetrahedral site in apatite is typically filled by phosphorus, although it may be substituted with other high-valence elements such as As and V (Fleet and Pan, 1994; Hughes and Rakovan, 2002; Piccoli and Candela, 2002; Hughes and Rakovan, 2015).

This study focuses on the Tampia gold deposit, located approximately 245 km east of Perth (Fig. 1) and hosted within high-grade metamorphic rocks of the Youanmi Terrane (Duuring, in press; Woad, 1988). Gold-bearing zones within mafic gneiss are characterized by the presence of abundant coarse-grained apatite genetically linked to gold mineralization. This study aims to determine whether apatite found within these ore zones possesses a distinct chemical signature compared to apatite present in less-mineralized mafic gneiss in the vicinity. If apatite in ore zones is found to possess a chemical signature indicative of gold mineralization, it could affirm its role as an effective medium for stream sediment sampling in the area, further enhancing its utility as a valuable tool for mineral exploration, particularly in the search for gold mineralization in the region.

Geological context

The Archean crystalline basement in the Yilgarn Craton primarily comprises granitic rocks (including granitic gneiss), with subordinate metamorphosed supracrustal rocks (ortho- and paragneiss, mafic and felsic volcanic rocks, quartzites, quartz–mica schists, and banded-iron formations) distributed throughout (e.g. Myers, 1993; Wilde et al., 1996; Cassidy et al., 2006). In the southern half of the western Yilgarn, supracrustal rocks form elongate, northwest-trending greenstone belts, while in the northern half they display variable geometries. The peak metamorphic grade exhibited by the supracrustal rocks ranges from granulite- and amphibolite-facies in the South West Terrane to amphibolite- and greenschist-facies further east and north in the Youanmi Terrane. The region has undergone multiple deformation and metamorphic events, including the Darling Orogeny (1205–1150 Ma), the Pinjarra Orogeny (1095–995 Ma), the Leeuwin Orogeny (780–515 Ma), and Mesozoic rifting-related deformation (Johnson, 2013).

The Tampia gold deposit was discovered in 1987 by BHP Minerals Pty Ltd as a result of identifying gold anomalism in regional bulk leach extractable gold (BLEG) stream samples (Woad, 1988). Before its operational phase, from late 2021 to mid-2023, the deposit had a combined resource of 11.318 million tonnes at an average grade of 1.91 grams per tonne (g/t) of gold (Au), yielding a total of 695,500 ounces (oz). This resource included an indicated 9.948 million tonnes at 1.94 g/t Au (620,500 oz) and an inferred 1.370 million tonnes at 1.7 g/t Au (75,000 oz) (Explaurum Limited, 2017).

The geological setting in the district is complex, elucidated through a combination of exploration practices, including drilling, along with airborne and ground magnetic and gravity surveys (Woad, 1988). The region is predominantly composed of felsic gneiss interspersed with narrower bands of mafic gneiss and metamorphosed banded-iron formation, all of which have been folded and metamorphosed under upper-amphibolite to granulite-facies conditions. Peak metamorphic conditions are estimated at 7.7 – 8.8 kbar and 795–835 °C, with an apparent thermal gradient between 95 °C/kbar and 103 °C/kbar (De Paoli et al., 2024). North-trending granitic plutons, approximately 3 × 2 km in size, intrude the folded gneisses (Duuring, 2024). Proterozoic east–west trending dolerite dykes up to 50 m wide and tens of kilometres long traverse the district geology, cutting the folded gneisses and granitic plutons.

Methods

Sample selection

To investigate apatite's potential in recording the chemical signature of an ore-bearing hydrothermal fluid, a selection of samples representing apatite from typical mafic gneiss and ore mineral-bearing veins and leucosomes were collected for detailed petrological study and bulk rock geochemical analysis. The typical mafic gneisses are medium-grained, equigranular, plagioclase- and pyroxene-rich and have a low abundance of sulfide minerals. Conversely, samples taken from veins and leucosomes are distinguished by abundant coarse-grained sulfides and arsenides and are associated with significantly higher gold concentrations (>1 ppm).

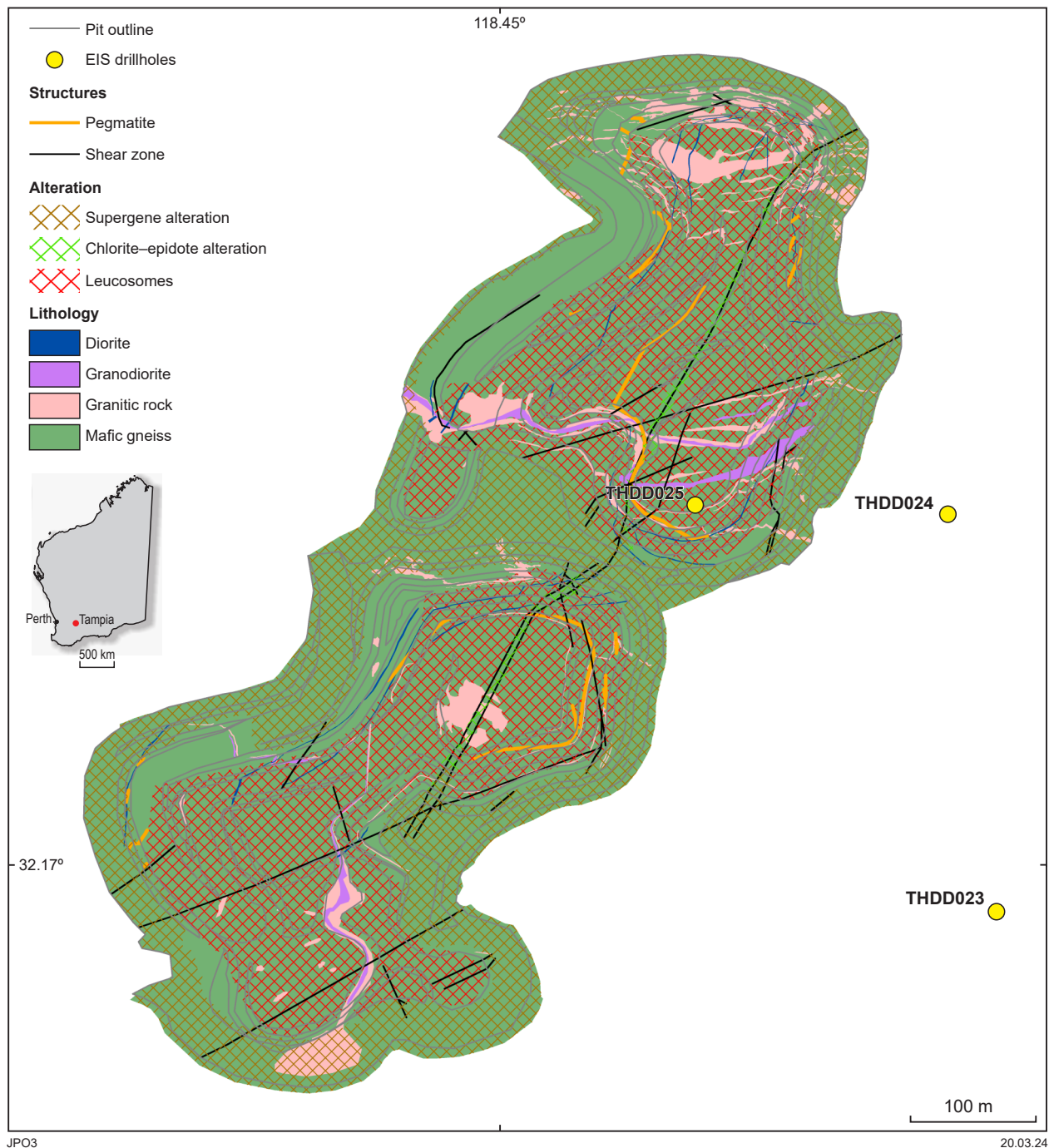


Figure 1. An interpreted solid geology map for the Tampia gold deposit, showing the location of the sampled drillholes

Three drillholes funded by the Exploration Incentive Scheme (EIS) – THDD023, THDD024 and THDD025 (Fig. 1; detailed in Appendix 1) were drilled to investigate the depth extent of the Tampia gold ore body. These drillholes were logged to obtain a comprehensive understanding of the geological context. Samples representing the typical mafic gneiss, plus the narrower gold-mineralized leucosomes and veins within these drillholes (Fig. 2) were collected for the preparation of 53 polished thin sections. From these, 15 were selected for detailed analysis using the TESCAN Integrated Mineral Analyzer (TIMA). These analyses focused on assessing the major and minor mineral constituents within the samples. The aim was to determine the mineralogical and textural variations between the mafic gneiss wallrock and the more mineralized veins and leucosomes in the gneiss, and to

assess the presence and characteristics of apatite within these samples.

TIMA

Polished thin sections were analysed using the TIMA at the John de Laeter Centre (JdLC), Curtin University. The TIMA is a high-resolution field emission scanning electron microscope with four fully integrated energy dispersive spectroscopy (EDS) detectors designed for automated mineralogical mapping. Samples were analysed using the liberation analysis and dot mapping modes with a 3 micrometre (μm) pixel size (Hrstka et al., 2018). Operating conditions of 25 kiloelectronvolts (keV) were selected

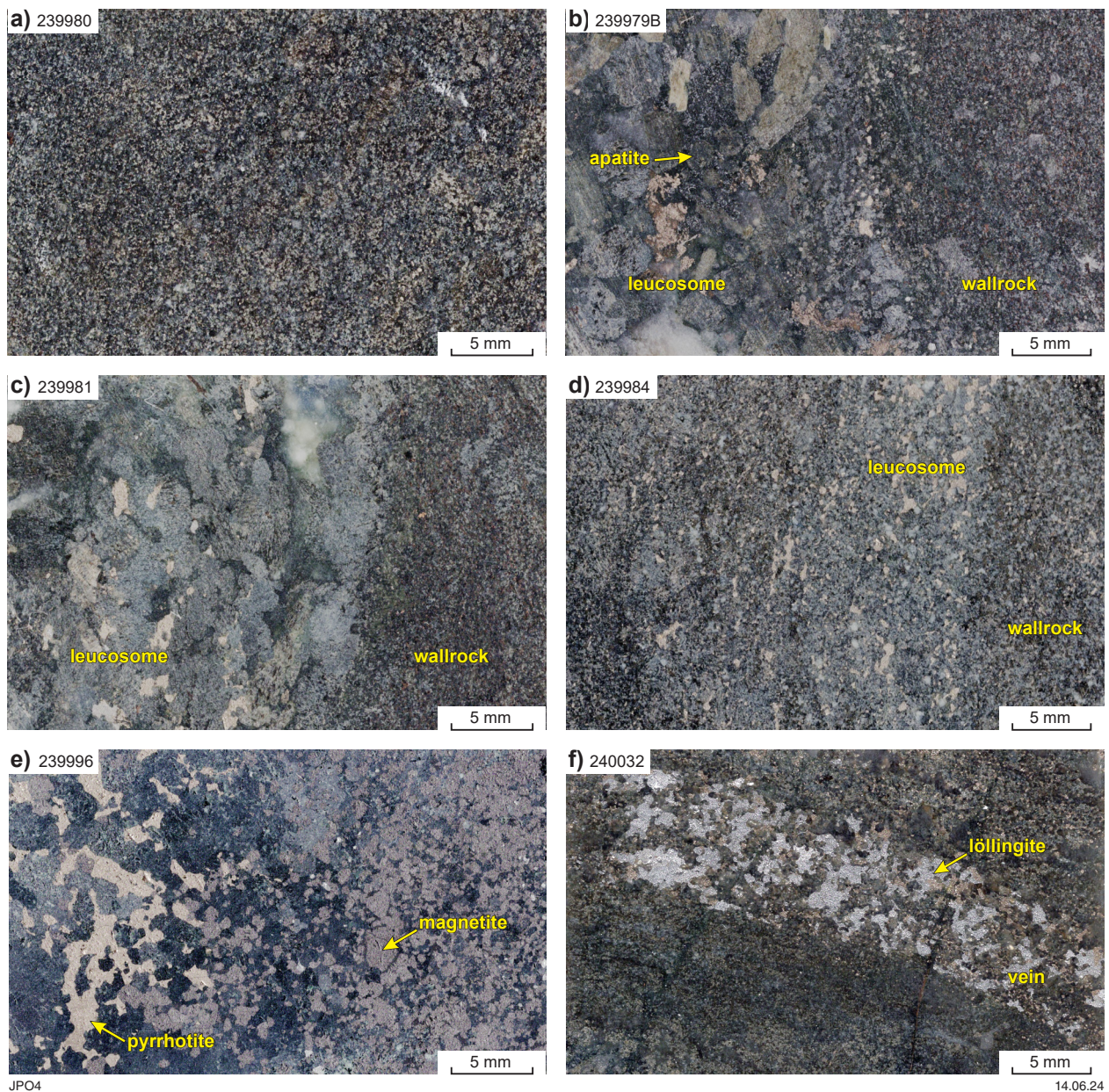


Figure 2. Photographs of mafic gneiss: a) typical mafic gneiss; b–f) gold-bearing examples of mafic gneiss, locally expressed as coarser-grained leucosomes or veins

using a spot size of 18.6 nanometres (nm), a working distance of 15 mm and a field size set at 1500 mm. TIMA measurements combine EDS analyses with back-scattered electron (BSE) imaging to identify individual grains and their boundaries. The measured spectral information was compared to definition files within an in-house database of minerals in the TIMA software (V.2.8.0) to produce quantitative mineral maps of the thin sections.

EPMA

Electron probe microanalysis (EPMA) was conducted using the JEOL JXA-8530F at the University of Tasmania. Analyses were performed using a defocussed 5 μ m, 15 nanoampere (nA) electron beam with a 15 kilovolt (kV) accelerating voltage and carbon coating on the polished mounts. The microprobe is equipped with five wavelength-

dispersive crystal spectrometers, one JEOL silicon-drift energy-dispersive spectrometer and an optical microscope. Calibration was performed on certified synthetic and natural mineral standards.

Seventeen elements were measured: Si, Al, La, Ce, Nd, Fe, Mn, Mg, Ca, Sr, Na, K, P, S, As, Cl and F. The ZAF Model was used to correct for background matrix effects. Efforts were made to reduce migration of fluorine through the use of a defocussed electron beam and by analysing grains oriented perpendicular to the beam (Stormer et al., 1993; Stock et al., 2015). Despite these efforts, a few analyses exceeded the maximum F content possible in apatite – i.e. 3.77 weight percent (wt%) – and are considered endmember fluorapatites (Appendix 2).

LA-ICP-MS

Trace element analyses were completed using laser ablation inductively coupled plasma mass spectrometry (LA-ICP-MS) at The University of Western Australia using the methods of Fisher et al. (2020). A Teledyne Photon Machines Analyte G2 193 nm ArF excimer-based laser ablation system was employed in conjunction with a high-resolution (HR) sector-field Thermo Fisher Scientific™ Element™ XR HR-ICP-MS. Ablation was carried out using a 4 joules per centimetre (J/cm²) fluence and a 5 hertz (Hz) repetition rate. Spot sizes were maintained at 25, 30 or 40 µm depending on the apatite grain size (Appendix 3). Each analysis consisted of a 30-second gas blank, a 10-second laser warm-up period, followed by 60 seconds of ablation for a total of 300 laser pulses. Each analysis was followed by a 20-second washout period before the next analysis began.

Thirty-six isotopes were measured: ²⁵Mg, ²⁹Si, ³¹P, ⁴³Ca, ⁴⁵Sc, ⁴⁹Ti, ⁵²V, ⁵⁵Mn, ⁷⁵As, ⁷⁷Se, ⁸⁵Rb, ⁸⁸Sr, ⁸⁹Y, ⁹¹Zr, ⁹³Nb, ¹³⁷Ba, ¹³⁹La, ¹⁴⁰Ce, ¹⁴¹Pr, ¹⁴⁶Nd, ¹⁴⁷Sm, ¹⁵³Eu, ¹⁵⁷Gd, ¹⁵⁹Tb, ¹⁶³Dy, ¹⁶⁵Ho, ¹⁶⁶Er, ¹⁶⁹Tm, ¹⁷²Yb, ¹⁷⁵Lu, ¹⁸¹Ta, ²⁰⁶Pb, ²⁰⁷Pb, ²⁰⁸Pb, ²³²Th, ²³⁸U. Data reduction was completed using iolite v.4.8.2 Trace Elements data reduction scheme software (Paton et al., 2011). The US National Institute of Standards and Technology (NIST) glass standard NIST612 was the main reference material (<http://georem.mpch-mainz.gwdg.de>). Glass standard NIST610 and apatite standard MAD (Fisher et al., 2020) were used as secondary reference materials to assess data quality.

Results

TIMA analyses identified six samples from three drillcores containing apatite grains (>20 µm) suitable for EPMA and LA-ICP-MS analysis. These samples are taken from mafic gneiss, the primary host rock for gold at the Tampia gold deposit and exhibit varying degrees of obvious mineralization, veining and coarse-grained leucosomes.

Drillhole THDD025 (Fig. 1) serves as a key study site as it intersects the main gold mineralization corridor at the Tampia gold deposit and contains a notable ~4 m interval with two narrow mineralized zones bordered by wallrock mafic gneiss with no obvious mineralization. Three of the samples (239979B, 239980, 239981) are derived from within ~3 m of each other in drillhole THDD025 (87.37 – 91.43 m). Sample 239980 represents the typical mafic gneiss with no obvious mineralization; whereas, samples 239979B and 239981 both contain mineralized leucosomes and less obviously mineralized wallrock. Sample 239979B is 0.85 m above the typical mafic gneiss (239980); whereas, sample 239981 is 0.91 m downhole of it. Sample 239984, also from drillhole THDD025, ~123 m farther downhole (214.53 – 214.68 m), contains a narrow area of visible mineralization and represents a more distal ore zone in mafic gneiss, which may offer insights into deeper mineralogical variations.

Samples 239996 and 240032 were included to cover a wider spatial range and display clear mineralogical and bulk rock geochemical differences. Sample 239996 is from drillhole THDD024 (183.40 – 183.60 m), approximately 200 m east of THDD025, outside the main Tampia pit (Fig. 1). The most distal sample, 240032, was sampled from drillcore of THDD023 (206.22 – 206.27 m), approximately 300 m south of THDD024. This sample selection strategy aimed to test

the mineralogical diversity within the gold-rich ore zones and evaluate the impact of gold mineralization on the host mafic gneiss. Appendix 4 summarizes locations and descriptions of each sample.

Apatite morphology and mineral associations

Sample 239980, mafic gneiss

Sample 239980 represents a mafic gneiss with no obvious mineralized veining or leucosomes (Figs 2a, 3a). This sample exhibits a massive, equigranular texture of predominantly plagioclase, clinopyroxene and orthopyroxene and contains only trace amounts of fine-grained white mica, disseminated pyrrhotite and ilmenite, with lesser amounts of arsenopyrite, chalcopyrite and pyrite. The sample was assayed to have a gold content of <0.72 ppm (Franey, 2019), but no gold was observed in the thin section. A comprehensive description of this sample, including observations from hand specimen and TIMA analyses and petrological descriptions, is summarized in Appendix 5.

Within sample 239980, over 20 apatite grains with diameters exceeding 20 µm were identified as candidates for detailed mineral chemistry analysis. Apatite grains are predominantly round to ovoid and tabular shaped. These anhedral to subhedral grains are typically <50 µm in diameter. They are frequently located within the plagioclase groundmass and are also associated with pyroxene, including orthopyroxene and clinopyroxene. Less commonly, apatite grains are found adjacent to ilmenite and sulfides (Fig. 4a). Although not abundant compared to other samples in this dataset, the predominant sulfide in this rock sample is pyrrhotite (1 vol%), accompanied by trace amounts of arsenopyrite, löllingite (an iron arsenide), glaucodot (a cobalt–nickel löllingite group arsenopyrite), chalcopyrite and pentlandite.

Samples 239979B and 239981, mineralized leucosomes in mafic gneiss

Sample 239979B (Figs 2b, 3b), comprises two main zones: a very coarse-grained clinopyroxene–orthopyroxene-bearing leucosome; and a medium-grained plagioclase–clinopyroxene–orthopyroxene-bearing mafic gneiss similar to that of sample 239980. The leucosome features coarse-grained clinopyroxene and orthopyroxene (0.5 – 1 cm), which are variably altered to actinolite and chlorite, and occur together with quartz. Opaque minerals identified within the leucosome include ilmenite, pyrrhotite, arsenopyrite with associated löllingite, gold, scheelite (calcium tungstate), sphalerite and pentlandite. For a complete list of mineralogy and petrographic descriptions, see Appendix 3.

Apatite grains in sample 239979B were observed to be too small (<20 µm) to analyse from the mafic gneiss wallrock; therefore, all analyses from this sample are from apatite grains in the leucosome. Apatite grains in this sample are the largest observed in this dataset, typically presenting as rounded, subhedral forms; often exceeding 500 µm in size and typically associated with pyroxene (Fig. 4b). Notably, these apatite grains frequently contain rounded quartz inclusions ranging in size, up to 200 µm.

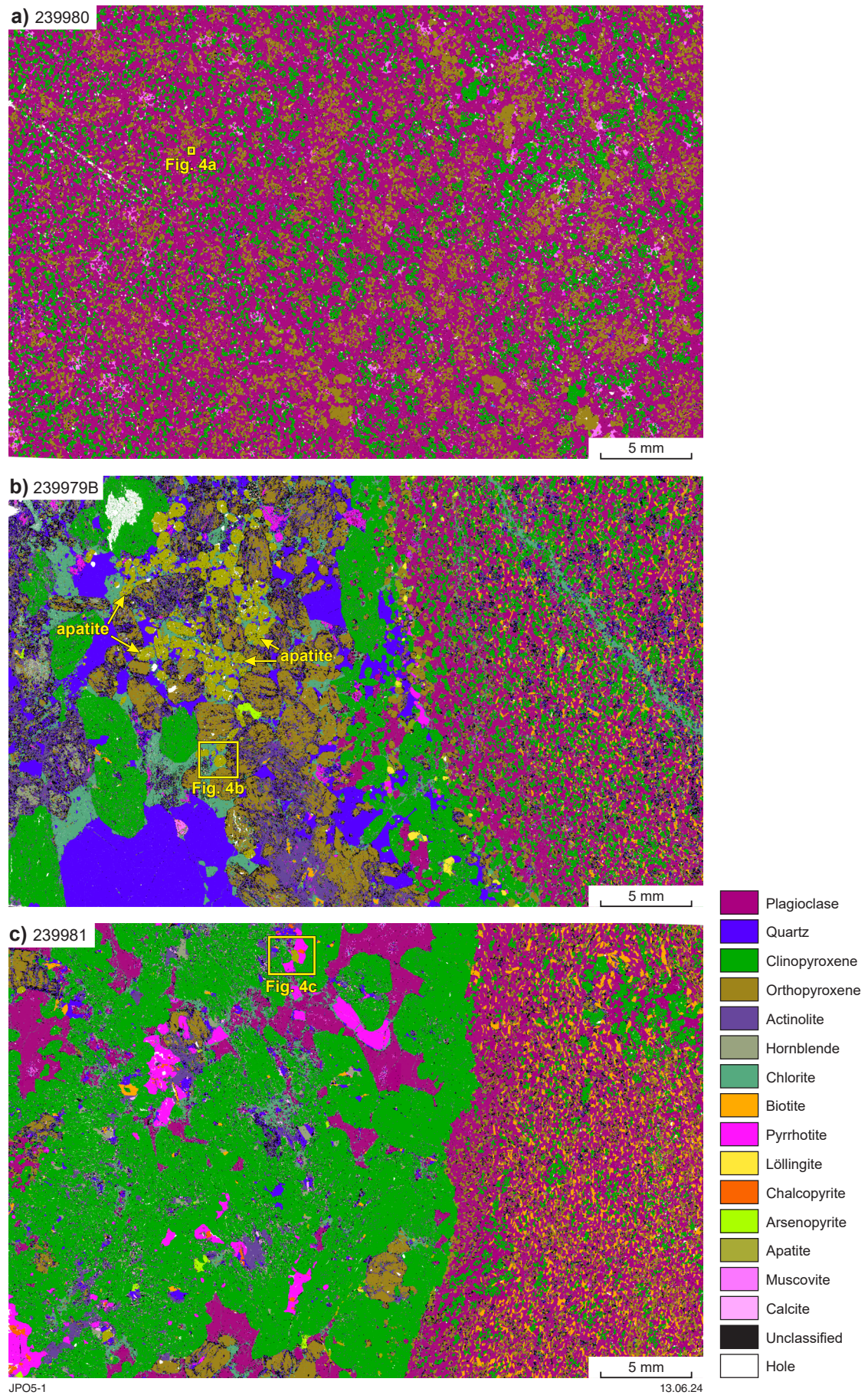


Figure 3. TIMA false-colour images of the polished sections of mafic gneiss examined by this study, demonstrating their textural and mineralogical distinctions: a) typical mafic gneiss; b–c) gold-bearing examples of mafic gneiss expressed as leucosomes with coarser-grained minerals

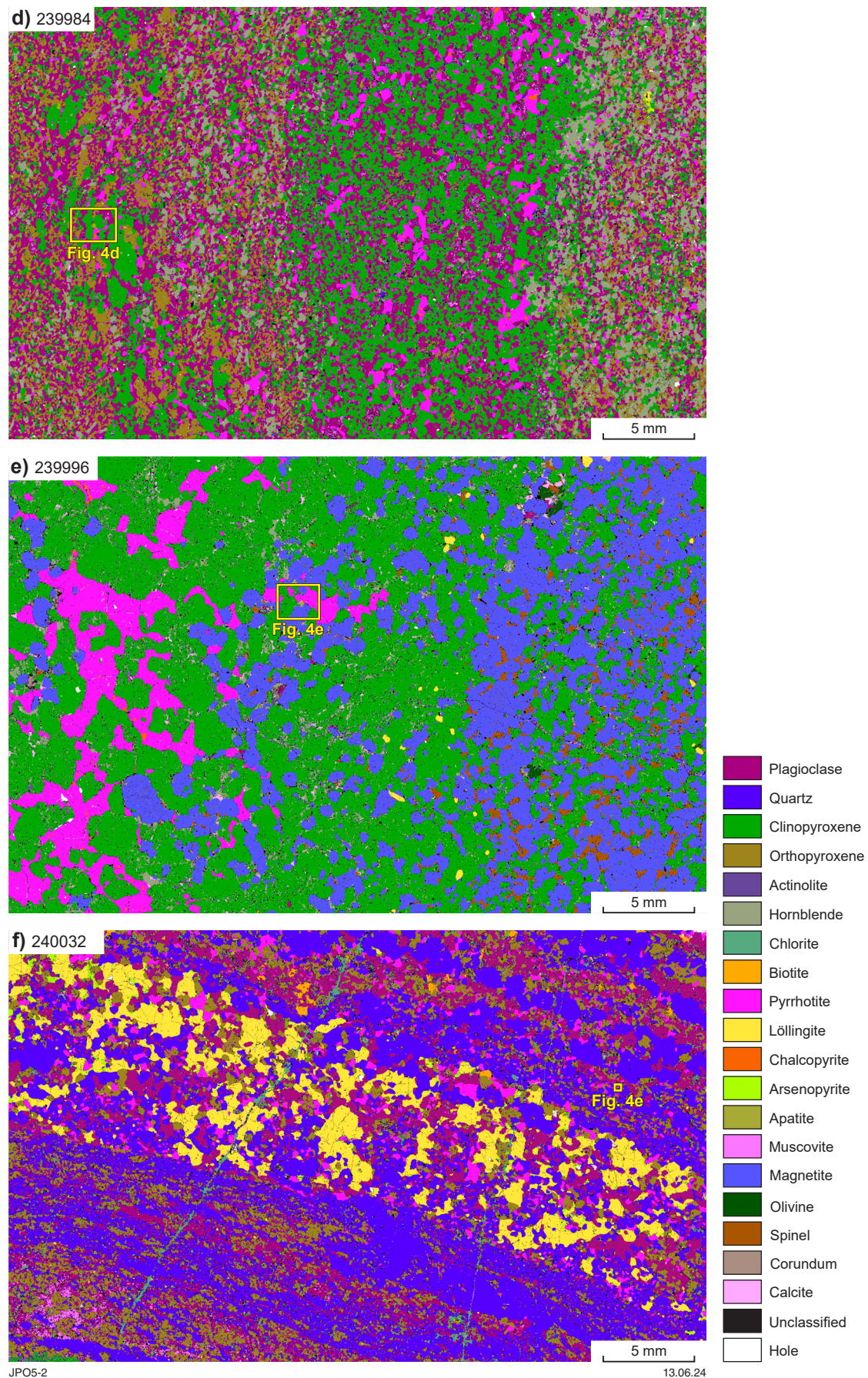


Figure 3. (cont.) TIMA false-colour images of the polished sections of mafic gneiss examined by this study, demonstrating their textural and mineralogical distinctions: d-e) gold-bearing examples of mafic gneiss expressed as leucosomes with coarser-grained minerals; f) metamorphosed vein

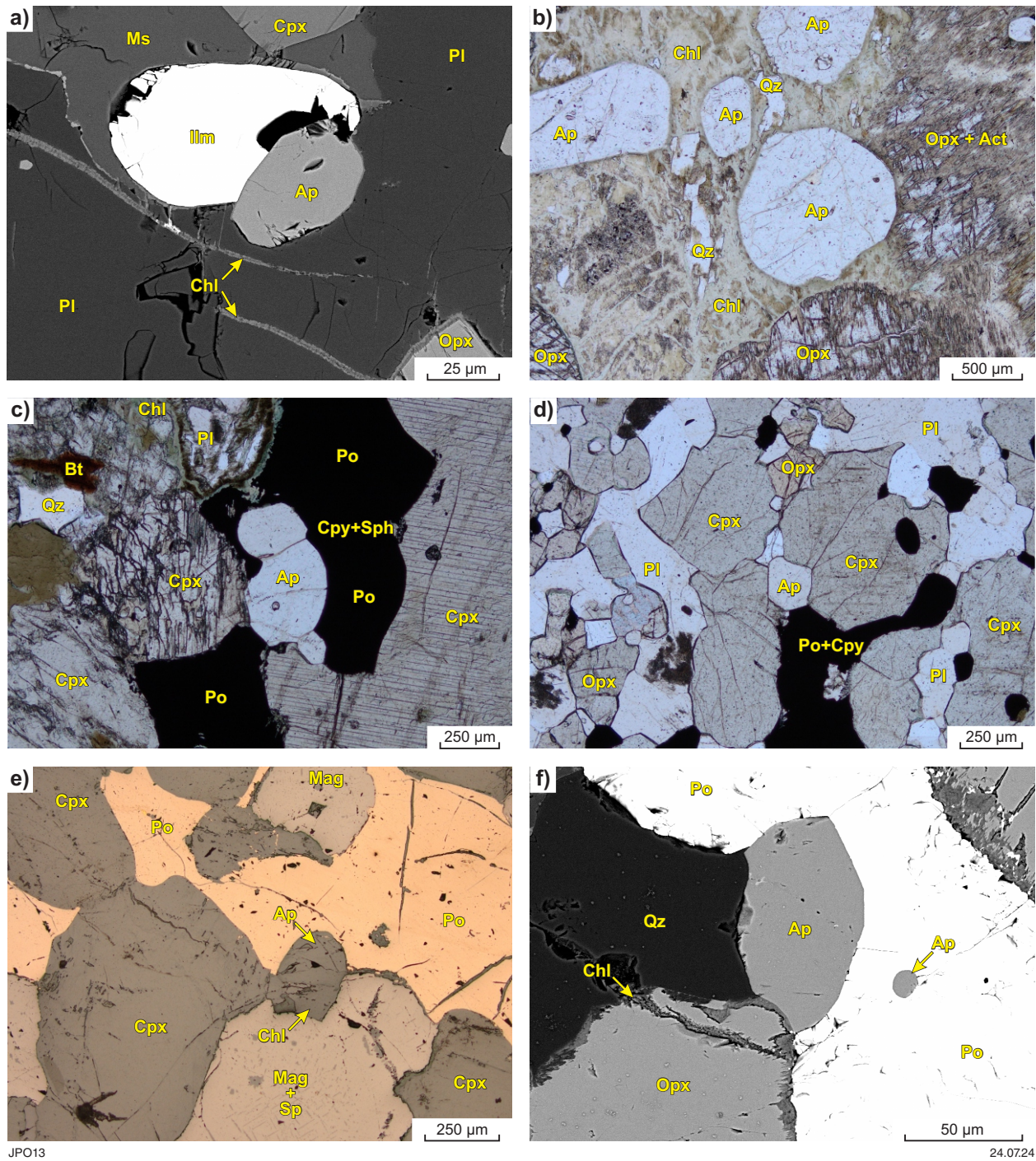


Figure 4. Photomicrographs of apatite grains in mafic gneiss: a) sample 239980, back-scattered electron (BSE) image of apatite with associated ilmenite and plagioclase, b) sample 239979B, plane-polarized light (PPL) image of rounded apatite in chlorite and orthopyroxene, c) sample 239981, PPL image of apatite intergrown with sulfides and clinopyroxene, d) sample 239984, PPL image of granoblastic mafic gneiss with apatite, sulfides and clinopyroxene, e) sample 239996, reflected light image of apatite and associated pyrrhotite, magnetite and clinopyroxene, f) sample 240032, BSE image of apatite intergrown with pyrrhotite and quartz. Abbreviations: Act – actinolite, Ap – apatite, Bt – biotite, Chl – chlorite, Cpy – chalcopyrite, Ilm – ilmenite, Mag – magnetite, Ms – muscovite, Opx – orthopyroxene, Pl – plagioclase, Po – pyrrhotite, Qz – quartz, Sp – spinel, Sph – sphalerite

Pyrrhotite and sphalerite are found as intergranular minerals between apatite grains, and there is one example of arsenopyrite intergrown within an apatite grain (Fig. 3b).

Sample 239981 (Figs 2c, 3c) also consists of a coarse-grained leucosome and adjacent medium-grained wallrock with similar mineralogy to the mafic gneiss of sample 239980. The wallrock of sample 239981 comprises medium-grained clinopyroxene, plagioclase, orthopyroxene and biotite laths. The leucosome is primarily composed of very coarse-grained (>1 cm) clinopyroxene, with interspersed plagioclase and orthopyroxene grains. Actinolite is associated with the breakdown of clinopyroxene and orthopyroxene, and chlorite is found at the boundaries of plagioclase. Associated mineralization appears in greater size and abundance within the leucosome, and includes pyrrhotite, with minor amounts of chalcopryite, arsenopyrite, löllingite, sphalerite, glaucodot, scheelite and gold (see Appendix 5). Apatite grains are primarily located in the coarse-grained, clinopyroxene-rich leucosome in the thin section.

Apatite grains within the wallrock of the mafic gneiss of sample 239981 were too small for LA-ICP-MS analysis; therefore, all textural and mineralogical observations pertain solely to the apatite grains found in the leucosome. Apatite grains are large, up to 500 µm in length (Fig. 4c) and display a range of shapes, from kidney-like and anhedral (as inclusions within clinopyroxene) to tabular and elongate, often forming at the boundaries of other minerals, especially clinopyroxene and, infrequently, pyrrhotite. Apatite grains are frequently located adjacent to ore minerals (Fig. 4c).

Sample 239984, mineralized leucosome in mafic gneiss

Sample 239984 (Figs 2d, 3d) is representative of a mineralized leucosome in mafic gneiss ~123 m downhole of the other samples from drillcore THDD025. This sample contains a central coarse-grained zone of poikiloblastic clinopyroxene, plagioclase and pyrrhotite bounded on either side of medium-grained, amphibole-rich mafic gneiss. The wallrock mineralogy is medium-grained, equigranular plagioclase, orthopyroxene and hornblende. Mineralization occurs in both the leucosome and wallrock zones as pyrrhotite, chalcopryite, arsenopyrite, löllingite, sphalerite, scheelite and gold (Appendix 5). Arsenopyrite is commonly a replacement texture after löllingite.

The apatite grains within sample 239984 are found both inside the leucosome and the wallrock mafic gneiss, indicating a varied distribution and mineral association. However, as apatite grains are larger within the leucosome, most analyses were performed on grains in this zone. The apatite grains are predominantly rounded, anhedral and the majority are <100 µm. They are closely associated with pyroxenes, less frequently plagioclase, and share grain boundaries with sulfides (Fig. 4d).

Samples 239996 and 240032, mineralized samples from other drillholes

Sample 239996 (Figs 2e, 3e), located in a distal drillhole (THDD024), is atypical in this dataset as it comprises magnetite, spinel, corundum and olivine. The thin section

of this sample is bimodal: one side is a coarse-grained clinopyroxene, pyrrhotite and magnetite; the other consists mainly of medium-grained clinopyroxene, magnetite, spinel (as magnetite inclusions and at magnetite grain triple junctions) and olivine. Löllingite occurs as coarse, spherical grains throughout, and chalcopryite occurs as inclusions within the pyrrhotite. Other opaque minerals include sphalerite, arsenopyrite, scheelite and gold.

In sample 239996, apatite grains were analysed in both the coarse-grained clinopyroxene–pyrrhotite zone and magnetite–clinopyroxene–spinel zone. Apatite ranges in size, from subhedral grains of approximately 300 µm in intergranular spaces, to anhedral inclusions of ~20 µm within magnetite. Apatite grains are commonly inclusions in magnetite within the magnetite-rich zone and share grain boundaries with pyroxene, magnetite, pyrrhotite and, less frequently, plagioclase elsewhere (Fig. 4e). This sample is distinctive as it has the only visibly chemically zoned apatite in this dataset.

Sample 240032, from drillhole THDD023, is the most distal from the main Tampia pit and is from an intensely mineralized zone, containing 2.51 ppm Au (Franey, 2019). The thin section is taken across a vein comprised mainly of coarse-grained, anhedral löllingite, in association with pyrrhotite, plagioclase, orthopyroxene and chalcopryite. Löllingite commonly displays rims of arsenopyrite, and gold is found at the interface of these two minerals. The wallrock contains plagioclase–orthopyroxene–quartz-rich bands that define the rock fabric. Orthopyroxene grains are poikiloblastic, with plagioclase and quartz inclusions.

Apatite grains were analysed predominantly in the wallrock of sample 240032 (Figs 2f, 3f); however, two grains were analysed within the löllingite vein. Generally, the apatite in this sample is <50 µm in size (Fig. 4f), although a few grains are ~200 µm in length. Outside the vein, many apatite grains are associated with quartz, plagioclase and pyrrhotite; whereas within the vein, they are commonly associated with löllingite, arsenopyrite and pyroxene.

Apatite chemistry

Samples 239980, 239979B, 239981

Apatite from the typical wallrock mafic gneiss of sample 239980 exhibits characteristic chondrite-normalized REE multi-element trends typical for gabbros, showcasing high total REE contents, negative slopes indicative of the relative enrichment of light REE (LREE) over heavy REE (HREE), alongside significant negative Eu anomalies (Fig. 5a). Compared with apatite from closely situated samples (within ~3 m) 239979B and 239981, the REE trends observed are remarkably similar. They exhibit comparable chondrite-normalized REE multi-element trends (Fig. 5a) and demonstrate similar anomalies for Y, Eu and Ce (Figs 6a, 6b). Employing the Sr/Y vs sum LREE discrimination graph proposed by O'Sullivan et al. (2020), these samples are classified as high-grade metamorphic rocks with a basic igneous compositional source (Fig. 7).

The three samples exhibit low Cl levels, with sample 239981 containing less than 0.1 wt%, while samples 239979B and 239980 average 0.23 wt% (Fig. 6c). The apatite grains exhibit

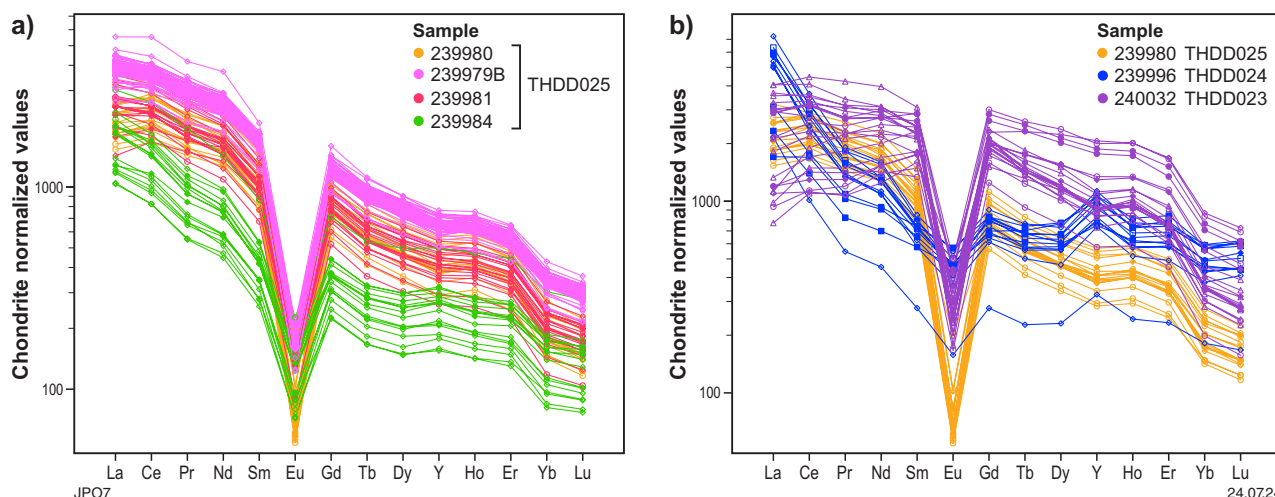


Figure 5. Multi-element plots displaying REE and Y contents in apatite from mafic gneiss: a) trend comparison between samples from drillhole THDD025; b) comparison of multi-element trends between mafic gneiss samples from drillhole THDD025 and mineralized samples from drillholes THDD023 and THDD024. Values normalized to chondrite according to Sun and McDonough (1989)

comparable values of As and V, (generally <100 ppm and <10 ppm, respectively) which can substitute for P in apatite (Fig. 8a). Similarly, Mn and Sr contents are low across all three samples, with most samples having <600 ppm Mn and <200 ppm Sr (Fig. 8b). In contrast, sample 239979B exhibits a slightly increased Th content (Fig. 8c) compared to the other two samples from drillhole THDD025, accompanied by a corresponding decrease in P and Ca contents (Fig. 8d).

These findings highlight the consistent geochemical signatures and anomalies in the apatite analyses, regardless of location in relation to visible mineralization, which underscores their similar origin and the influence of metamorphic and igneous processes on their composition. The slight variations in Th, P and Ca contents among the samples may reflect localized differences in the original composition of the source rocks, or in the fluid or alteration conditions.

Sample 239984

Sample 239984, located ~123 m below the other three samples analysed in drillhole THDD025, exhibits distinct geochemical characteristics in its apatite compositions. This distally located and mineralized (3.5 ppm Au; Franey, 2019) mafic gneiss sample contains apatite grains with lower total REE contents compared to the other samples (Fig. 5a). It also exhibits intermediate negative Ce and Eu anomalies, as illustrated in Figures 6a and 6b. Despite the lower total REE contents, the chondrite-normalized REE trends remain similar across all samples, characterized by comparable total REE fractionation trends, as evidenced by overlapping (Ce/Yb)_N values (Fig. 6d). However, this sample is distinguished by higher (La/Sm)_N values, indicating slightly steeper negative LREE slopes compared to the other three samples (Figs 5a, 6d), as well as more pronounced positive Y anomalies (Figs 5b, 6a).

When classified using the Sr/Y vs sum LREE contents, these apatite grains are indicative of those of a high-grade metamorphic origin (Fig. 7). The halogen content of sample 239984 aligns with that of apatite grains from samples within the same drillhole (Fig. 6c), as Cl contents are

<0.1 wt%, and F contents (>3.00 wt%) approach endmember values for fluorapatite. The P and Ca contents are high, showing overlapping ranges with samples 239980 and 239981 (Fig. 8d). Both Th and U contents are notably low at <40 ppm and <25 ppm, respectively (Fig. 8c). Significantly, As contents are higher in sample 239984, averaging approximately 225 ppm (Fig. 8a).

These observations highlight the nuanced differences in apatite geochemistry between distally located mineralized samples and their counterparts at shallower depths in the same drillhole.

Samples 239996 and 240032

Samples 239996 (drillhole THDD024) and 240032 (drillhole THDD023) are mineralized samples with notable gold contents: 2.17 ppm and 2.51 ppm, respectively (Fray, 2019). These samples exhibit distinct mineral assemblages compared to those from drillhole THDD025, with 239996 being a magnetite-rich leucosome in mafic gneiss and 240032 featuring a löllingite-rich vein within mafic gneiss. These samples were chosen for comparison due to their mineralized nature and differing ore mineral assemblages, providing a contrast to the samples analysed in THDD025 and insights into the variability of mineralization and host rock types across spatially distinct locations.

Sample 240032 (löllingite-rich vein) shares similar chemistry with the THDD025 samples but differs from sample 239996 (magnetite-rich leucosome) in overall REE trends (Fig. 5b) and (Ce/Yb)_N vs (La/Sm)_N relationships (Fig. 6d). It shows a positive LREE slope, with depletion in La and Ce relative to Sm, unlike the other samples, and a flat-to-weakly negative total REE slope (Figs 5b, 6d). However, Y, Eu, and Ce anomalies are similar to the THDD025 samples (Fig. 6a,b). Chemical distinctions are more pronounced in halogens and other trace element contents, with 240032 having the lowest F (<2.45 wt%) and highest Cl (up to 1.59 wt%) contents among all analysed samples (Fig. 6c). It also displays lower As, V, Th, P and Ca contents and moderately high Mn and Sr contents (Fig. 8).

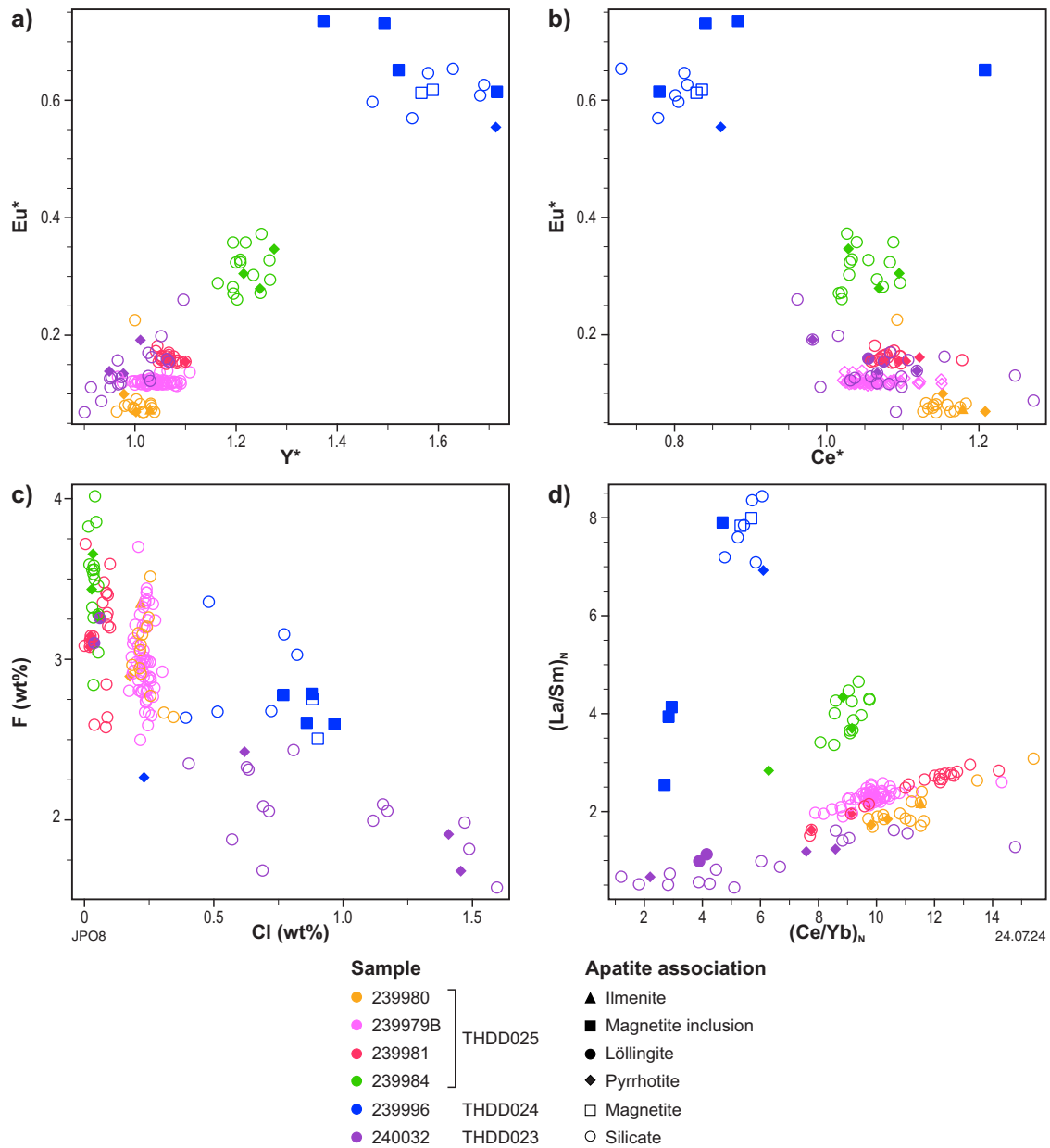


Figure 6 Binary plots used to discriminate between compositional groups of apatite in mafic gneiss: a) Y^* vs Eu^* ; b) Ce^* vs Eu^* ; c) Cl vs F ; d) $(Ce/Yb)_N$ vs $(La/Sm)_N$. The following formulae and abbreviations are noted: $(Ce/Yb)_N = (Ce/0.957)/(Yb/0.248)$, $(La/Sm)_N = (La/0.367)/(Sm/0.231)$, $Y^* = (Y/2.1)/\sqrt{[(Dy/0.381)*(Ho/0.0851)]}$, $Eu^* = (Eu/0.087)/\sqrt{[(Sm/0.231)/(Gd/0.306)]}$, $Ce^* = Ce/0.957/[(La/0.367)^{(2/3)}*(Nd/0.711)^{(1/3)}]$. The diagrams were generated using ioGAS™ software, adhering to the methodology outlined by Taylor and McLennan (1985)

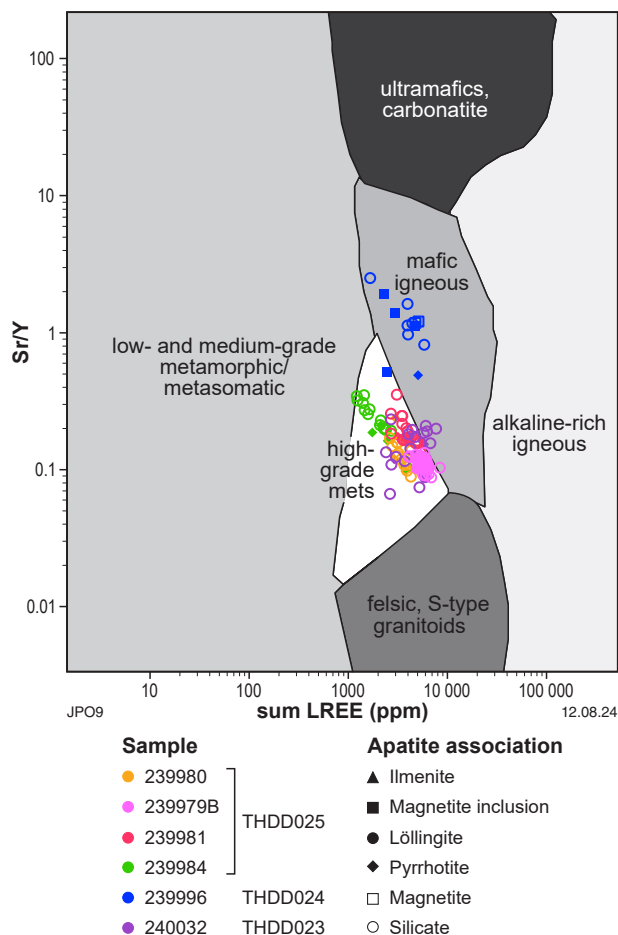


Figure 7. Apatite source discrimination diagram: sum LREE (ppm) vs Sr/Y; where sum LREE = La + Ce + Pr + Nd + Sm, following the methodology described by O'Sullivan et al. (2020)

Association with löllingite influences apatite chemistry, particularly regarding U, P and Ca, contents (Figs 8c, 8d); whereas Cl contents are lower and F contents are higher, akin to apatite found in the THDD025 samples (Fig. 6c). The apatite grains are classified as belonging to high-grade metamorphic rocks with a basic igneous composition using the Sr/Y vs sum LREE discrimination graph (Fig. 7).

Sample 239996, a magnetite-rich leucosome, exhibits the most distinct geochemistry in the dataset, including a subtle negative Eu anomaly (Fig. 5b), a pronounced positive Y anomaly (Fig. 6a) and a negative Ce anomaly (Fig. 6b). Its REE plot shows a steeply negative LREE slope and a flat-to-positive HREE slope (Fig. 5b), placing it within the basic igneous zone on the discrimination diagram (Fig. 7). Halogen contents are intermediate, with Cl averaging 0.71 wt% and F ranging from 2.26 wt% to 3.36 wt% (Fig. 6c). Phosphorus content is low (<17.9 wt%), while As, Mn, Sr and Th contents are the highest among the dataset (Fig. 8).

Apatite inclusions in magnetite exhibit distinct chemistry, particularly in the LREE slope (Fig. 6d) and Y and Ce anomalies (Figs 6a, 6b), along with Th and P contents, although these differences vary between inclusions. Trace element chemistry also differs in apatite grains associated with pyrrhotite, especially in Cl/F ratios (Fig. 6c), highlighting the complex interplay of mineral associations and geochemical signatures in these mineralized samples.

Discussion

Apatite as an indicator of host rock compositional variability

This research primarily aims to explore the potential of apatite chemistry in gold exploration, with a secondary focus on its ability to differentiate host rock types. The congruence in geochemical tracers (i.e. Cr, Co and Ni) from Tampia whole-rock geochemistry (Fig. 9), commonly used to compare and classify mafic and ultramafic rocks (Hastie et al., 2007; Barnes et al., 2014), suggests these samples originated from identical precursor host rocks, indicating a consistent geological context for mineral chemistry analysis. This hypothesis was validated by apatite mineral chemistry, which shows that apatite from the typical mafic gneiss and from mineralized leucosomes and veins all exhibit similar REE patterns and immobile trace element concentrations, affirming the effectiveness of apatite in mirroring original, pre-mineralizing fluid, host rock geochemistry within THDD025.

Contrastingly, when comparing mafic gneisses from drillholes THDD023 and THDD024, which exhibit distinct whole-rock immobile element ratios, their apatite chemistry also reveals divergent REE patterns and trace element (e.g. Cl, F, P, Th, Mn, Sr and As) values. This indicates that subtle variations in the original host rocks are captured in their apatite compositions, even though these precursor rocks underwent granulite-facies metamorphism, leading to recrystallization and granoblastic textures. Consequently, apatite proves to be a reliable indicator of host rock variability, effectively preserving the geochemical signatures of their original geological settings.

Evaluating apatite's utility in identifying gold mineralization

Our investigation aimed to determine apatite's effectiveness in signalling gold mineralization by analysing the chemistry of apatite from both typical, apparently unmineralized, wallrock mafic gneiss samples and those that are mineralized, containing veins and leucosomes. The focus was on drillhole THDD025 due to its unique positioning, offering a comparative analysis between apatite grains from wallrock mafic gneiss, leucosomes and veins in close proximity, as well as from a mineralized, more distal sample within the same drillhole, and additional samples from drillholes THDD023 and THDD024 farther afield.

Despite notable differences in mineralogy, texture and whole-rock geochemistry between the apatite grains, the chemistry was uniform across most sample types. They generally shared similar REE patterns; showcased equivalent europium anomalies (Eu*); and had comparable ratios of LREE to HREE. Additionally, the concentration of more mobile elements such as As, V, Mn and Sr in the apatite remained consistent across the samples.

This chemical homogeneity implies that apatite does not effectively differentiate between apatite grains found in different parts of the mineralizing system within the background mafic gneiss. The inability of apatite to exhibit distinct chemical signatures between these sample types at the Tampia gold deposit could be attributed to several factors:

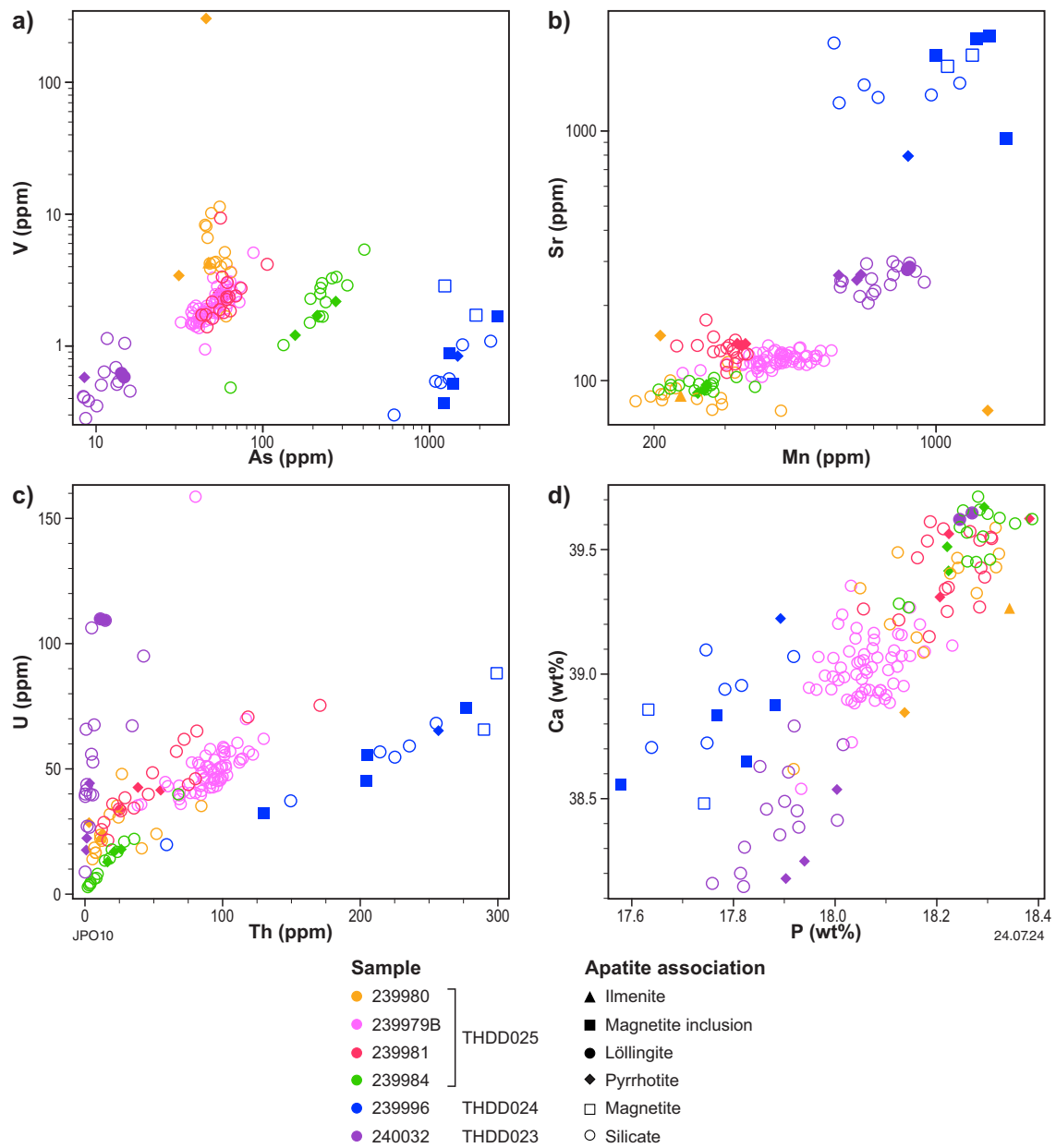


Figure 8. Binary plots used to discriminate between compositional groups of apatite in the mafic gneiss: a) As vs V; b) Mn vs Sr; c) Th vs U; d) P vs Ca

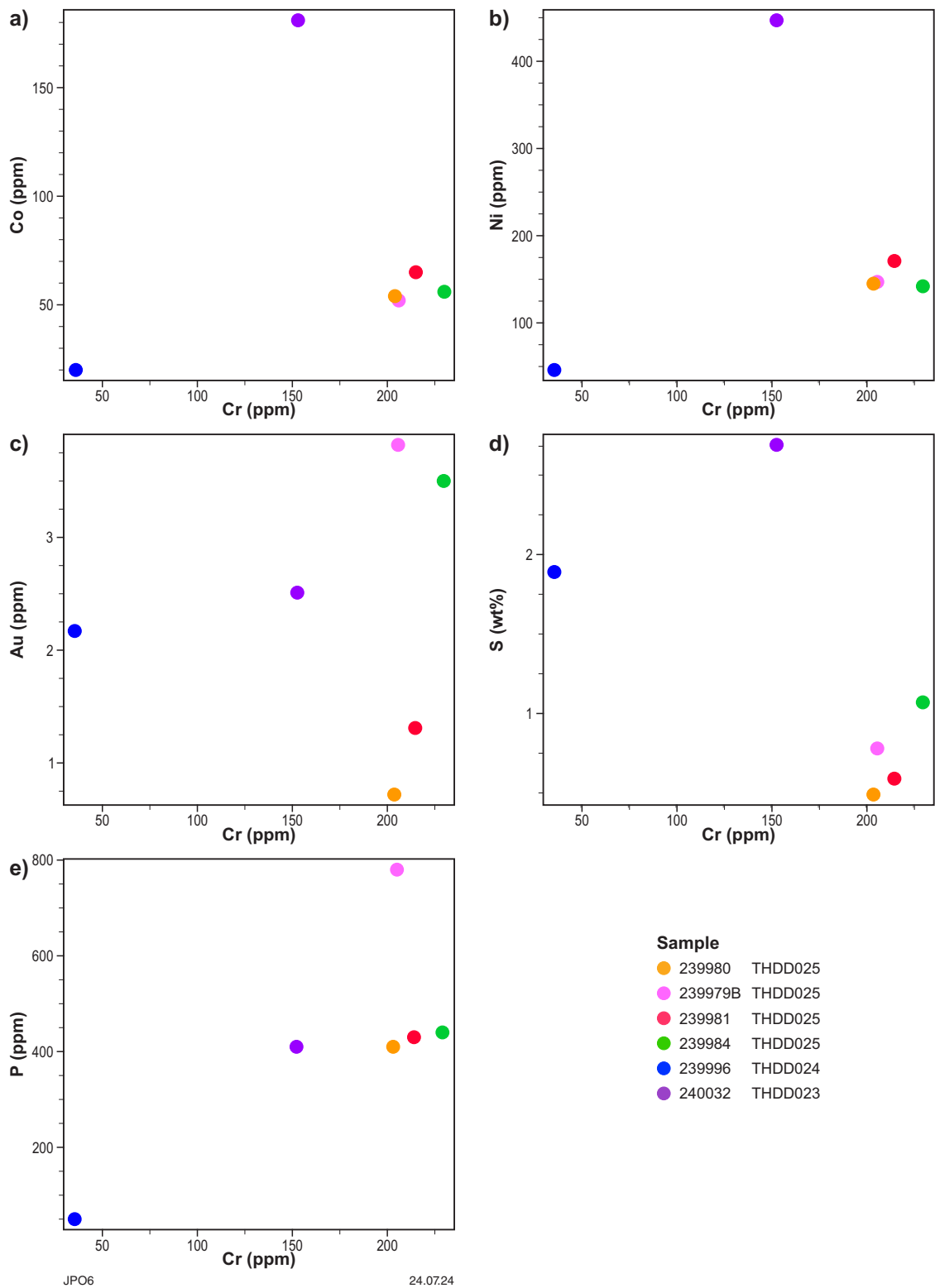


Figure 9. Bulk rock trace element geochemistry of mafic gneiss samples from the Tampia gold deposit. This figure displays the geochemical profiles of selected samples, focusing on geochemical tracers for mafic and ultramafic rocks (Cr vs Co, Cr vs Ni) (Hastie et al., 2007; Barnes et al., 2014), as well as Au, S and P contents. Samples 239980, 239979B, 239981 and 239984 show similar immobile element ratios, ideal for direct apatite mineralogy comparison. Conversely, samples 239996 and 240032, from distal drillholes, exhibit different ratios, highlighting the apatite chemistry diversity in gold-bearing zones. Notably, the typical mafic gneiss sample, 239980, has the lowest Au and S levels, while P content of the samples is varied

- (1) **Mineralizing fluids affected apatite grains within the wallrock mafic gneiss:** the apparent uniformity in apatite chemistry may be due to most apatite grains being exposed to mineralizing fluids regardless of location, compromising the possibility of using certain grains as pre-mineralization benchmarks. This is supported by the significantly higher gold concentration (0.72 ppm over 0.33 m) found within the wallrock mafic gneiss when compared to the crustal average (0.004 ppm), according to Rudnick and Gao (2003). The detection of ore-related minerals (löllingite, sphalerite, scheelite, glaucodot, chalcopyrite) not visible in initial examinations of the typical mafic gneiss further corroborates that the 'benchmark' sample at Tampia underwent similar ore processes to visibly mineralized samples. This suggests all samples are potentially mineralized and future studies should seek out genuine unmineralized mafic gneiss from outside the mineralized corridor for accurate comparison of apatite compositions, alongside global dataset analyses for better contextual understanding (this latter suggestion has been attempted below).
- (2) **Homogenization of apatite chemical signatures by metamorphic conditions:** another possibility is that apatite grains were initially varied due to differing exposures to mineralizing fluids, but their chemical signatures became uniform under granulite-facies metamorphic conditions. Such conditions could erase initial trace element diversity, making it challenging to discern original environmental differences. If true, this homogeneity would be consistent across all apatite compositions regardless of their associations with nearby minerals, grain size and morphology, or proximity to leucosomes enriched in Si, S and As. Nevertheless, evidence indicates that a complete homogenization has not occurred, as distinct chemical trends in apatite that reflect whole-rock composition differences are preserved.
- (3) **Natural limitations of apatite as a geochemical indicator due to ionic compatibility:** the third consideration stems from the intrinsic limitations of apatite to act as a geochemical indicator for gold mineralization in granulite-facies rocks. Whole-rock geochemical data (Franey, 2019) for the examined drillholes establishes a positive correlation between Au and various elements in mineralized mafic gneiss, demonstrating strong correlations with As, Ag and Sb, and weaker or localized associations with W, Bi, Cd, Cu, Zn, Mo and S. The integration of these elements into the crystal structure of apatite is constrained by their ionic radius and charge, which naturally limits the compatibility of many pathfinder elements associated with gold mineralization. Among these, only As and S are compatible with the apatite structure, highlighting a significant limitation in using apatite to directly detect indicators of mineralization. It suggests that elements tied to gold mineralization are more likely to be found in other minerals, such as sulfides, arsenides and scheelite, rather than in apatite.

Comparison of Tampia apatite with regional apatite compositions

In this investigation, the apatite chemistry database created by Mao et al. (2016) was employed, which encompasses data from both barren and mineralized host rocks of magmatic–hydrothermal ore deposits, to conduct a comparative analysis of Tampia apatite grains with worldwide instances of mineral deposits. Using discriminant projection analysis with a focus on the elements Mn, Sr, Y, La, Ce, Eu, Dy, Yb, Pb, Th and U, the bulk of Tampia samples were categorized as 'unmineralized rocks', in alignment with the Mao et al. (2016) established criteria (Fig. 10a). Advancing with the classification scheme proposed by Mao et al. (2016), specific Tampia apatite samples that were classified as 'ore deposits'; namely, 239980 and 239984, underwent reclassification into the Au \pm Co/Cu/Pb–Zn skarns category (Fig. 10b).

Although this classification appears significant, the inherent challenge in the Mao et al. (2016) method to not consistently recognize actual gold-bearing samples from Tampia as 'ore deposit' samples reveals a significant drawback of the classification system. This issue indicates that the existing database may not possess suitable analogues for Tampia apatite samples, implying that the designation of the Tampia mineral system as an Au \pm Co/Cu/Pb–Zn skarn highlights this classification scheme is not accurate with regard to this deposit and should be regarded with caution.

The recent work by Fisher et al. (2023) focuses on using zircon and apatite from both barren and mineralized igneous samples to identify metallogenic fertility markers within Archean terranes of the Yilgarn and Pilbara Cratons in Western Australia. Their database predominantly consists of samples from barren igneous rock suites unrelated to any known gold mineralization and includes samples from various 'intrusion-related' (Lang and Baker, 2001) and orogenic gold deposits (Groves et al., 1998). The intrusion-related deposits are hosted in igneous rocks, with some deriving gold directly from felsic magmatic sources. The orogenic gold deposits, with their structurally controlled gold zones, are not genetically linked to their felsic magmatic hosts, such as the syenite-hosted Jupiter gold deposit in the Yilgarn Craton (Duuring et al., 2000).

Fisher et al. (2023) report that apatite grains from mineralogically fertile suites exhibit distinctive REE patterns that are smooth, with high La/Yb ratios and no Eu anomaly ($\text{Eu}/\text{Eu}^* > 0.5$). Additionally, these apatite grains have elevated S (300–4000 ppm) and Sr (>1000 ppm) concentrations. By these specific criteria, none of the samples from the Tampia gold deposit would be considered fertile. Only one sample (239996 from drillhole THDD024) demonstrated Sr values exceeding 1000 ppm and an Eu anomaly greater than 0.5 ppm (Fig. 11a). Furthermore, S values in the Tampia samples did not reach 300 ppm, with most analyses showing S concentrations below 100 ppm. These low S contents displayed by Tampia apatite grains deviate from trends defined for 'fertile' apatite from porphyry Cu–Mo systems (Xu et al., 2021). This variation in S contents at Tampia, coupled with the observation of gold grains within löllingite, suggests that As might serve as a more accurate fertility discriminant than S for the Tampia gold deposit. Figure 11b demonstrates that apatite from this dataset, apart from the most distal sample 240032, often have As contents >40 ppm and many contain more As than S.

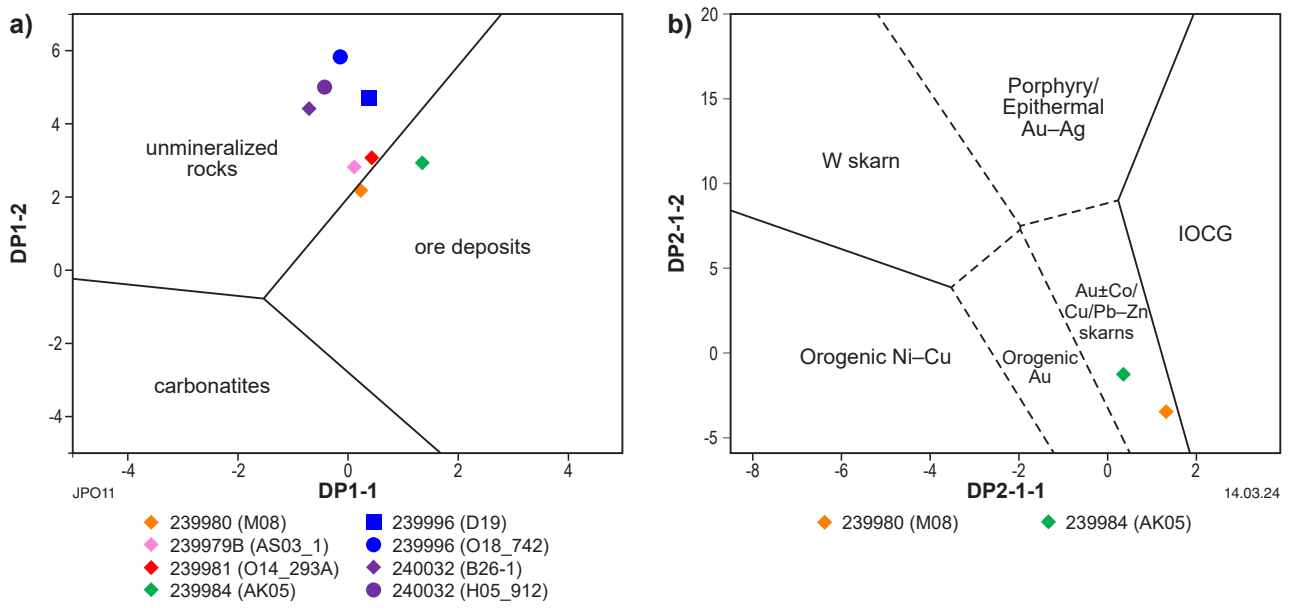


Figure 10. A method for discriminating mineralization potential and categories based on apatite chemistry across global deposit examples: a) A plot showing representative analyses from each apatite sample (Appendix 3), using the discrimination algorithm developed by Mao et al. (2016); b) A plot illustrating representative analyses from apatite samples classified as originating from an 'ore deposit', applying the second step of the discrimination algorithm by Mao et al. (2016)

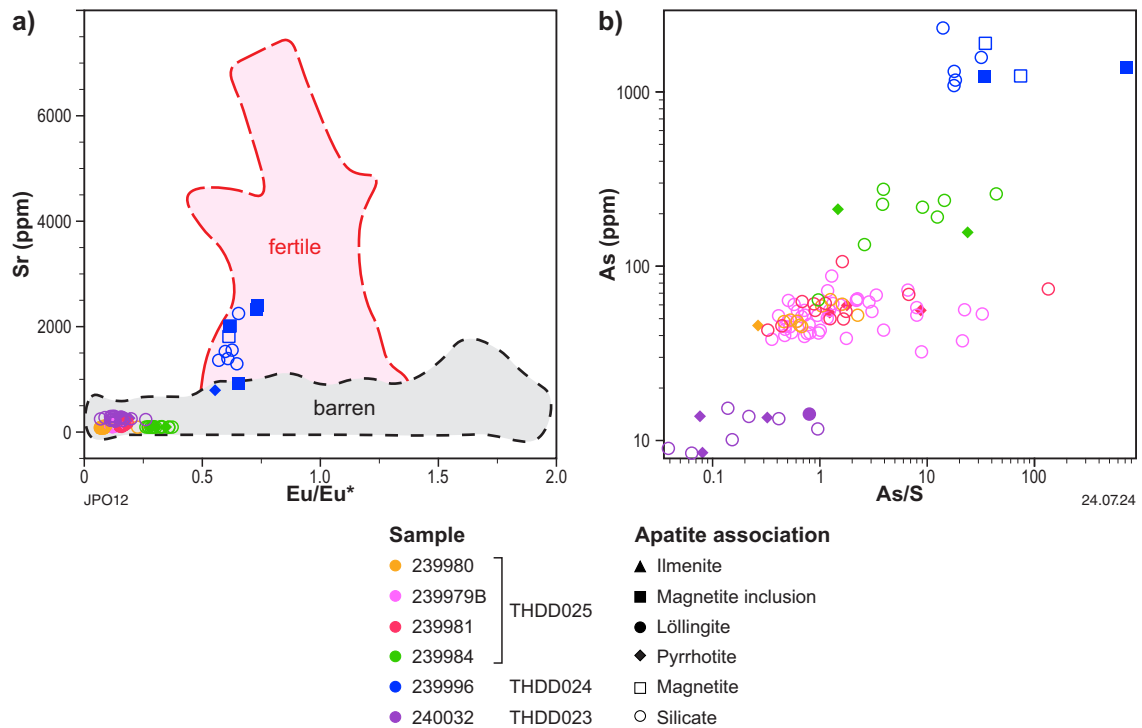


Figure 11. a) Rock fertility discrimination diagram from barren and mineralized sample of the Yilgarn Craton, after Fisher et al. (2023); b) As vs As/S

The observed discrepancy between the chemical characteristics of Tampia apatite and established fertility indicators for the Yilgarn and Pilbara Cratons can be attributed to several potential explanations:

- (1) Apatite at Tampia did not form during the gold mineralization event, despite now being preserved proximal to ore minerals.
- (2) If the apatite grains were contemporaneous with gold mineralization, any chemical signature indicative of this event might have been obliterated through the homogenization of apatite by fluids reflective of a barren, high- P – T metamorphic environment.

Or:

- (3) A significant limitation may lie within the existing geochemical databases, which lack examples of granulite-facies gold deposits hosted by mafic rocks, similar to Tampia. This gap in the data may inadvertently contribute to the misclassification or misunderstanding of the geochemical signatures observed at Tampia.

Conclusions

This study aimed to evaluate the efficacy of apatite chemistry as a discriminant between mineralized rocks with different degrees of alteration within granulite-facies metamorphosed terranes, specifically at the Tampia gold deposit. The findings can be summarized as follows:

- (1) **Mirroring of host rock compositional variations:** apatite chemistry successfully mirrored the inherent compositional differences in host rocks. Mafic gneisses, regardless of apparent fluid alteration and sharing identical precursor rock signatures, exhibited congruent apatite chemistry trends. This included similar chondrite normalized REE patterns, anomalies for Eu, Ce and Y, and trace element abundances for Cl, F, Sr and Mn. In contrast, apatite grains from mafic gneisses across different drillholes; and thus, potentially different source-rock chemistry, showed distinct whole-rock immobile element ratios, as well as divergent apatite compositions.
- (2) **Lack of distinction in mineralized samples:** apatite from obviously mineralized samples at Tampia could not be reliably distinguished from apatite located in the typical wallrock mafic gneiss as they lack consistent mineralization trends in REE, halogens, and trace elements. This is likely due to the near ubiquitous penetration of mineralizing fluids within the ore zone, rendering apatite in wallrock a poor benchmark for comparison to apatite with a clear association with ore mineralogy.

- (3) **Comparison with global and Western Australian datasets:** the Tampia samples did not fit well within the global classification system designed for a variety of mineral deposits, as outlined by Mao et al. (2016), nor did they exhibit the fertile trends identified by Fisher et al. (2023) for the Yilgarn and Pilbara Cratons.

- (4) **Possible explanations for the observations:** the absence of recognizable fertility signatures in Tampia apatite samples may result from limitations in the regional databases; the possibility that Tampia apatite grains did not crystallize contemporaneously with gold mineralization; or the homogenization of any mineralization-related chemical signature by barren, high- P – T metamorphic fluids.

- (5) **Recommendations for further research:** future work should explore the impact of primary lithological controls on apatite chemistry at Tampia by incorporating data from different host rocks, obtaining genuinely unmineralized samples for comparison and conducting comparative analyses with other similar metamorphosed gold deposits located within the southwest Yilgarn Craton, such as Griffins Find and those defining the Katanning goldfield.

In conclusion, the disparity between Tampia apatite chemistry and the established fertility markers for the Yilgarn and Pilbara Cratons highlights the challenges of interpreting mineral chemistry data in mineral exploration. This underscores the need for a detailed approach that accounts for geological history, mineral formation timing and the potential alteration of apatite by metamorphic processes. Moreover, it emphasizes the importance of expanding and refining geochemical databases to encompass a wider range of deposit types and geological settings; thereby, improving the predictive capabilities of mineralogical and geochemical indicators in gold exploration.

Acknowledgements

We are thankful to the GSWA, MRIWA, Anglo American Ltd, Ramelius Resources Ltd. and CSIRO for their support of this work through the MRIWA 10433 Project. Many thanks to Chris Fisher for assistance with the LA-ICP-MS; Karsten Goemann and Sandra Romano for assistance with the EMPA; and Imogen Fielding for assistance with TIMA data processing.

References

- Barnes, SJ, Fisher, LA, Anand, R and Uemoto, T 2014, Mapping bedrock lithologies through in situ regolith using retained element ratios: a case study from the Agnew–Lawlers area, Western Australia: *Australian Journal of Earth Sciences*, v. 61, p. 269–285.
- Belousova, EA, Kostitsyn, YA, Griffin, WL, Begg, GC, O'Reilly, SY and Pearson, NJ 2010, The growth of the continental crust: Constraints from zircon Hf-isotope data: *Lithos*, v. 119, no. 3–4, p. 457–466.
- Cao, M, Li, G, Qin, K, Seitmuratova, EY and Liu, Y 2012, Major and Trace Element Characteristics of Apatites in Granitoids from Central Kazakhstan: Implications for Petrogenesis and Mineralization: *Resource Geology*, v. 62, no. 1, p. 63–83, doi:10.1111/j.1751-3928.2011.00180.x.
- Cassidy, KF, Champion, DC, Krapež, B, Barley, ME, Brown, SJA, Blewett, RS, Groenewald, PB and Tyler, IM 2006, A revised geological framework for the Yilgarn Craton, Western Australia: Geological Survey of Western Australia, Record 2006/8, 8p.
- Chu, MF, Wang, KL, Griffin, WL, Chung, SL, O'Reilly, SY, Pearson, NJ and Iizuka, Y 2009, Apatite Composition: Tracing Petrogenetic Processes in Transhimalayan Granitoids: *Journal of Petrology*, v. 50, no. 10, p. 1829–1855, doi:10.1093/petrology/egp054.
- De Paoli, MC, Blereau, ER, Korhonen, FJ, Kelsey, DE and Fielding, IOH 2024, 219854: hornblende metagabbro, Merino prospect; Metamorphic History Record 31: Geological Survey of Western Australia, 8p., <www.dmirs.wa.gov.au/metamorphic-history>
- Duuring, P in press, Geological mapping of the Tampia gold deposit – overview and list of components: Geological Survey of Western Australia, Record 2024/4, 20p.
- Duuring, P 2024, 3D geological model for Tampia gold deposit – overview and list of components: Geological Survey of Western Australia; 3D Geomodel Series, <www.demirs.wa.gov.au/3Dgeoscience>.
- Duuring, P, Hagemann, SG and Groves, DI 2000, Structural setting, hydrothermal alteration, and gold mineralisation at the Archaean syenite-hosted Jupiter deposit, Yilgarn craton, Western Australia: *Mineralium Deposita*, v. 35, p. 402–421.
- Explarum Limited 2017, Significant increase for Tampia mineral resource to 700,000oz gold: Australian Securities Exchange (ASX), 26p.
- Fisher, CM, Bauer, AM, Luo, Y, Sarkar, C, Hanchar, JM, Vervoort, JD, Tapster, SR, Horstwood, M and Pearson, DG 2020, Laser ablation split-stream analysis of the Sm-Nd and U-Pb isotope compositions of monazite, titanite, and apatite – Improvements, potential reference materials, and application to the Archean Saglek Block gneisses: *Chemical Geology*, v. 539, article no. 119493, https://doi:10.1016/j.chemgeo.2020.119493.
- Fisher, CM, Kemp, AIS, Hagemann, SG, Lu, Y and Smithies, RH 2023, The use of zircon and apatite as metallogenic fertility indicators in Archean orogenic gold systems, in Target 2023 abstract volume edited by H McFarlane, G Begg and R Montison: Geological Survey of Western Australia, Record 2023/14, p. 16, 18p.
- Fleet, ME and Pan, Y 1994, Site preference of Nd in fluorapatite [$\text{Ca}_{10}(\text{PO}_4)_6\text{F}_2$]: *Journal of Solid State Chemistry*, v. 112, no. 1, p. 78–81.
- Franey, D 2019, Tampia Gold Project EIS co-funded Deep Diamond Drilling (R#16): Explarum Operations Pty Ltd: Geological Survey of Western Australia, Statutory mineral exploration report A119888, <www.dmirs.wa.gov.au/wamex>, 18p.
- Gillespie, J, Glorie, S, Khudoley, A and Collins, AS 2018, Detrital apatite U-Pb and trace element analysis as a provenance tool: Insights from the Yenisey Ridge (Siberia): *Lithos*, 314–315, p. 140–155, doi:10.1016/j.lithos.2018.05.026.
- Groves, DI, Goldfarb, RJ, Gebre-Mariam, M, Hagemann, SG and Robert, F 1998, Orogenic gold deposits: A proposed classification in the context of their crustal distribution and relationship to other gold deposit types: *Ore Geology Reviews*, v. 13, no. 1–5, p. 7–27.
- Harlov, DE 2015, Apatite: A Fingerprint for Metasomatic Processes: *Elements (Quebec)*, v. 11, no. 3, p. 171–176, doi:10.2113/gselements.11.3.171.
- Hastie, AR, Kerr, AC, Pearce, JA and Mitchell, SF 2007, Classification of Altered Volcanic Island Arc Rocks using Immobile Trace Elements: Development of the Th–Co Discrimination Diagram: *Journal of Petrology*, v. 48, no. 12, p. 2341–2357.
- Hrstka, T, Gottlieb, P, Skála, R, Breiter, K and Motl, D 2018, Automated mineralogy and petrology – applications of TESCAN Integrated Mineral Analyzer (TIMA): *Journal of Geosciences*, v. 63, no. 1, p. 47–63, doi:10.3190/jgeosci.250.
- Hughes, JM and Rakovan, J 2002, The Crystal Structure of Apatite, $\text{Ca}_5(\text{PO}_4)_3(\text{F},\text{OH},\text{Cl})$: *Reviews in Mineralogy and Geochemistry*, v. 48, no. 1, p. 1–12.
- Hughes, JM and Rakovan, JF 2015, Structurally Robust, Chemically Diverse: Apatite and Apatite Supergroup minerals: *Elements*, v. 11, no. 3, p. 165–170, https://doi:10.2113/gselements.11.3.165.
- Johnson, SP 2013, The birth of supercontinents and the Proterozoic assembly of Western Australia: Geological Survey of Western Australia, Perth, Western Australia, 78p.
- Krneta, S, Ciobanu, CL, Cook, NJ, EHRIG, K and Kontonikas-Charos, A 2017, Rare Earth Element Behaviour in Apatite from the Olympic Dam Cu–U–Au–Ag Deposit, South Australia: *Minerals*, v. 7, no. 8, p. 135, https://doi:10.3390/min7080135.
- Lang, JR and Baker, T 2001, Intrusion-related gold systems: The present level of understanding: *Mineralium Deposita*, v. 36, no. 6, p. 477–489.
- Mao, M, Rukhlov, AS, Rowins, SM, Spence, J and Coogan, LA 2016, Apatite trace element compositions: A robust new tool for mineral exploration: *Economic Geology*, v. 111, no. 5, p. 1187–1222.
- Myers, JS 1993, Precambrian history of the Western Australian Craton and adjacent orogens: *Annual Review of Earth and Planetary Sciences*, v. 21, p. 453–485, https://doi.org/10.1146/annurev.earth.21.050193.002321
- O'Sullivan, G, Chew, D, Kenny, G, Henrichs, I and Mulligan, D 2020, The trace element composition of apatite and its application to detrital provenance studies: *Earth-Science Reviews*, v. 201, article no. 103044, https://doi.org/10.1016/j.earscirev.2019.103044
- Paton, C, Hellstrom, JC, Paul, B, Woodhead, J and Hergt, J 2011, Iolite: Freeware for the Visualisation and Processing of Mass Spectrometric Data: *Journal of Analytical Atomic Spectrometry*, v. 26, p. 2508–2518, https://doi.org/10.1039/C1JA10172B
- Piccoli, PM and Candela, PA 2002, Apatite in Igneous Systems: *Reviews in Mineralogy and Geochemistry*, v. 48, no. 1, p. 255–292, https://doi.org/10.2138/rmg.2002.48.6
- Rudnick, RL and Gao, S 2003, Composition of the Continental Crust: *Treatise on Geochemistry*, v. 3, p. 1–64, https://doi.org/10.1016/B0-08-043751-6/03016-4
- Sha, L-K and Chappell, BW 1999, Apatite chemical composition, determined by electron microprobe and laser-ablation inductively coupled plasma mass spectrometry, as a probe into granite petrogenesis: *Geochimica et Cosmochimica Acta*, Vol. 63, no. No. 22, p. 3861–3881, https://doi.org/10.1016/S0016-7037(99)00210-0
- Stock, MJ, Humphreys, MCS, Smith, VC, Johnson, RD and Pyle, DM 2015, New constraints on electron-beam induced halogen migration in apatite: *American Mineralogist*, v. 100, no. 1, p. 281–293, https://doi.org/10.2138/am-2015-4949.

- Stormer, JC, Pierson, ML and Tacker, RC 1993, Variation of F and Cl X-ray intensity due to anisotropic diffusion in apatite during electron microprobe analysis: *American Mineralogist*, v. 78, p. 641–648.
http://www.minsocam.org/ammin/AM78/AM78_641.pdf
- Sun, S.-s and McDonough, WF 1989, Chemical and isotopic systematics of oceanic basalts: implications for mantle composition and processes, *in* *Magmatism in the Ocean Basins edited by* AD Saunders and MJ Norry: The Geological Society of London, Special Publication 42, p. 313–345.
<https://doi.org/10.1144/GSL.SP.1989.042.01.19>
- Taylor, SR and McLennan, SM 1985, *The Continental Crust: Its Composition and Evolution*: Blackwell Scientific Publications, Oxford, U.K., 312p.
- Wilde, SA, Middleton, MF and Evans, BJ 1996, Terrane accretion in the southwestern Yilgarn Craton: evidence from a deep seismic crustal profile: *Precambrian Research*, v. 78, p. 179–196,
[https://doi.org/10.1016/0301-9268\(95\)00077-1](https://doi.org/10.1016/0301-9268(95)00077-1)
- Woad, GM 1988, Tampia Hill, Annual Report, E70/463, July 1987 to August 1988: BHP Minerals Pty Ltd: Geological Survey of Western Australia, Statutory mineral exploration report 26815*,
<www.dmirs.wa.gov.au/wamex>, 946p., unpublished.
- Xu, B, Hou, Z-Q, Griffin, WL, Zhou, Y, Zhang, Y-F, Lu, Y-J, Belousova, E, Xu, J-F and O'Reilly, SY 2021, Elevated Magmatic Chlorine and Sulfur Concentrations in the Eocene–Oligocene Machangqing Cu–Mo Porphyry Systems: SEG Special Publications, v. 2, no. 24, p. 257–276. <https://doi.org/10.5382/SP.24.14>

APATITE CHEMISTRY AS A POSSIBLE INDICATOR
OF MINERALIZATION AT THE GRANULITE-FACIES
METAMORPHOSED TAMPPIA GOLD DEPOSIT

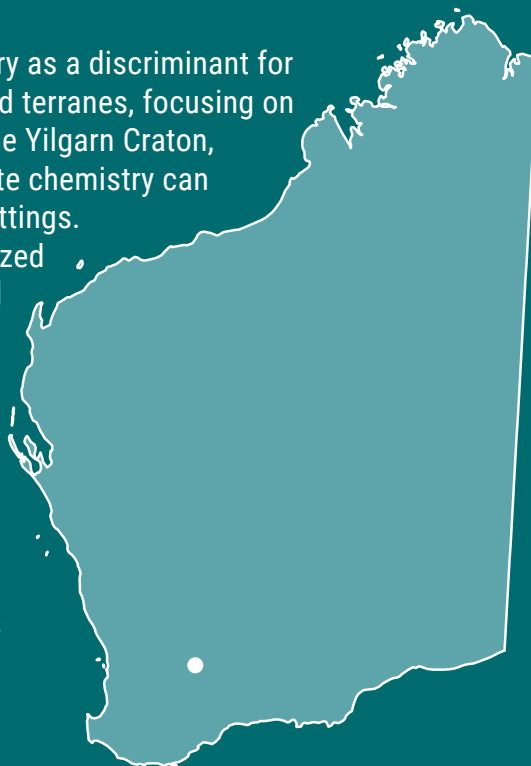
JK Porter and P Duuring

This report investigates the utility of apatite chemistry as a discriminant for mineralization within granulite-facies metamorphosed terranes, focusing on the Tampia gold deposit in the Youanmi Terrane of the Yilgarn Craton, Western Australia. The aim was to determine if apatite chemistry can identify gold mineralization in complex geological settings. Apatite grains from typical mafic gneiss and mineralized samples were analysed and compared against global and regional databases.

Results show that apatite chemistry at Tampia mirrors host rock compositions, with similar rare earth element trends and trace element abundances between wallrock and mineralized samples. However, mineralized samples did not exhibit distinguishable chemistry from typical gneiss, suggesting that apatite from these rocks was similarly affected by mineralizing fluids, did not form during gold mineralization, or was homogenized by metamorphic fluids.

Comparisons with global databases highlighted challenges in categorizing Tampia apatite due to mismatched fertility indicators. The study recommends expanding sample scope and conducting comparative analyses with similar deposits to better evaluate apatite chemistry's predictive power in gold exploration.

The study presented in this metadata report is the result of a collaborative research project titled *Detection of Distal Footprints of Mineral Systems in the Southwest of Western Australia: Linking Basement and Cover (SOWETO)*. This project was conducted in collaboration with the Geological Survey of Western Australia, the Commonwealth Scientific and Industrial Research Organisation, the Minerals Research Institute of Western Australia, Anglo American Ltd, and Ramelius Resources Ltd.



Further details of geoscience products are available from:

First Floor Counter
Department of Energy, Mines, Industry Regulation and Safety
100 Plain Street
EAST PERTH WESTERN AUSTRALIA 6004
Phone: +61 8 9222 3459 Email: publications@demirs.wa.gov.au
www.demirs.wa.gov.au/GSWApublications